Benzodiazole-Based Covalent Organic Frameworks for Enhanced Photocatalytic Dehalogenation of Phenacyl Bromide Derivatives

Ming Wang , Jiaying Qian , Shenglin Wang , Zhongliang Wen * , Songtao Xiao * , Hui Hu , Yanan Gao *

Posted Date: 25 July 2024

doi: 10.20944/preprints202407.1981.v1

Keywords: Covalent organic frameworks; heteropore; heterogeneous photocatalysis; dehalogenation

Article

Benzodiazole-Based Covalent Organic Frameworks for Enhanced Photocatalytic Dehalogenation of Phenacyl Bromide Derivatives

Ming Wang [1], Jiaying Qian [1], Shenglin Wang [1], Zhongliang Wen [1,*], Songtao Xiao [2,*], Hui Hu [1] and Yanan Gao [1,*]

[1] Key Laboratory of Ministry of Education for Advanced Materials in Tropical Island Resources, Hainan University, No 58, Renmin Avenue, Haikou 570228, China; ygao@hainanu.edu.cn
[2] China Institute of Atomic Energy. Beijing 102413, China; xiao200112@163.com
* Correspondence: zhongliang.wen@ugent.be (Z.W.); xiao200112@163.com (S.X.); ygao@hainanu.edu.cn (Y.G.)

Abstract: Covalent organic frameworks (COFs) have garnered significant interest within the scientific community due to their distinctive ability to act as organic semiconductors responsive to visible light. This unique attribute makes them up-and-coming candidates for facilitating photocatalytic organic reactions. Herein, two donor-acceptor COFs, TPE-BSD-COF and TPE-BD-COF, have been designed and synthesized by incorporating electron-rich tetraphenylethylene and electron-deficient benzoselenadiazole and benzothiadiazole units into the framework through a Schiff-base polycondensation reaction. Both COFs exhibits exceptional crystallinity and enduring porosity. TPE-BSD-COF and TPE-BD-COF exhibit broad light absorption capabilities, narrow optical band gap, and low electrochemical impedance spectrum (EIS) levels, indicating that the two COFs are effective heterogeneous photocatalysts for the reductive dehalogenation of benzoyl bromide derivatives under blue LED irradiation. TPE-BSD-COF and TPE-BD-COF achieved a high photocatalytic yield of 98% and 95%, respectively, within only one hour.

Keywords: covalent organic frameworks; heteropore; heterogeneous photocatalysis; dehalogenation

1. Introduction

Over the past few years, the adoption of heterogeneous photocatalysis in the field of organic synthesis has gained substantial momentum. This technique is celebrated for its straightforward application, eco-friendly processes, and mild operational conditions. As such, it is widely regarded as an effective and sustainable strategy for the generation of high-value fine chemicals. [1–4] In this area of study, creating and developing photocatalysts with outstanding performance in the photocatalysis process continues to be a significant obstacle. To date, significant efforts have been dedicated to developing highly active photocatalysts, including inorganic semiconductor materials, [5,6] organometallic compounds, [7] and organic dye molecules. [8] All these materials exhibit strong light absorption and excellent redox characteristics when excited by light at appropriate wavelengths. In recent years, the development of novel photocatalysts has focused on polymeric systems, such as polyaniline (PANI), [9] polythiophene, [10,11] graphitic carbon nitride (g-C_3N_4), [12,13] polypyrrole (PPy), [14] and metal-organic frameworks (MOFs). [15–17] These heterogeneous photocatalysts have exhibited high catalytic activities in various organic transformations and have such advantages over homogeneous counterparts as low cost, easy separation, and high reusability. Covalently linked porous aromatic frameworks (PAFs) have emerged as a promising platform as metal-free and highly

 doi:10.20944/preprints202407.1981.v1

efficient photocatalysts and demonstrated tremendous potential in various organic syntheses under light irradiation conditions. [18,19]

Covalent organic frameworks (COFs) are constructed from organic building blocks under the guidance of reticular chemistry and exhibit intriguing aesthetic architectures and permanent porosity as a novel class of crystalline porous organic polymer materials. The unique advantage of COFs lies in their ease of structural and functional tuning. [20–23] Moreover, COFs offer high specific surface area, low density, and excellent physicochemical stability, positioning them as ideal materials for applications in adsorption, [24,25] sensing, [26,27] energy storage, [28] and heterogeneous catalysis. [29–31] Two-dimensional (2D) structures showcase regular columnar π-arrays and one-dimensional (1D) nanopores, arising from the stacked layers of 2D macromolecular sheets. These organized and conductive columns provide a prime route for the separation, diffusion, and movement of photogenerated electron-hole pairs. Therefore, from a structural perspective, photoactive 2D COFs can be strong candidates for optoelectronic materials and photocatalysts. [32,33] The pioneering work by Lotsch's group has reported a hydrazone-based 2D COF that catalyzed hydrogen production from water under visible light. [34] Nonetheless, limited research is available on applying 2D COFs as solid photocatalysts for organic compound formation. [35,36]

Benzoselenadiazole and benzothiadiazole compounds are renowned for their photosensitizing properties and are commonly utilized in organic light-emitting diodes (OLEDs) and photovoltaic cells. [37] Recently, the development of COFs incorporating benzoselenadiazole/benzothiadiazole units has surged, revealing exceptional photocatalytic capabilities. [38,39] Furthermore, heteropore COFs offer various advantages compared to COFs with uniform single porosity, however, there is a lack of reports on heteropore COFs. [40] In this work, we synthesized two heteropore COFs, namely TPE-BSD-COF and TPE-BD-COF, that were constructed by a photoactive benzoselenadiazole and benzothiadiazole as building block. The two COFs demonstrate an outstanding photocatalytic performance due to their high crystallinity, intrinsic porosity, and low EIS. Acting as a heterogeneous photocatalyst for the reductive dehalogenation of benzoyl bromide derivatives. Among them, the photocatalytic yield of the novel TPE-BSD-COF reached 98% in only one hour.

2. Materials and Methods

Materials: All chemical reagents, unless otherwise noted, were purchased directly from Aladdin and TCI without the need for further purification.

Synthesis of TPE-BSD-COF: 4,4',4'',4'''-(ethene-1,1,2,2-tetrayl)tetraaniline (TPE, 9.8 mg, 0.025 mmol) and 4,4'-(benzothiadiazole-4,7-diyl)dibenzaldehyde (BSD, 20.0 mg, 0.05 mmol) were taken in a seal tube and a mixture of *o*-DCB/*n*-butanol (2 mL, v/v 1/1) and 3M acetic acid (0.1 mL) was added into the tube. The tube was sonicated for five minutes and degassed via a freeze-pump-thaw process. Then, the tube was sealed and allowed the reaction to proceed at 120 °C for 3 days. The precipitate was collected, washed with THF, and dried under vacuum to yield a yellow COF powder in 79% isolated yield.

Synthesis of TPE-BD-COF TPE (0.025 mmol, 9.8mg) and 4,4'-(Benzothiadiazole-4,7-diyl)dibenzaldehyde (BD, 0.05 mmol, 17.8 mg) were taken in a seal tube. A mixture of *o*-DCB/*n*-butanol (2 mL, v/v 1/1) and 3M acetic acid (0.1 mL) was added into the tube. The mixture was sonicated for 5 minutes and then degassed via a freeze-pump-thaw process. The tube was sealed and allowed the reaction to proceed at 120 °C for 3 days. The precipitate was collected, washed with THF, and dried under vacuum to yield a yellow COF powder in 82% isolated yield.

Characterizations: All the reagents and solvents were of reagent grade and used as received. ^{1}H NMR spectra and ^{13}C NMR spectra were recorded on a Bruker DPX 400 spectrometer. Solid-state ^{13}C CP/MAS NMR was performed on a JNM-ECZ600R 600 MHz spectrometer with a 3.2-mm double-resonance MAS probe. The FT-IR spectra were obtained using a JASCO FT-IR-6800 Fourier transform infrared spectrophotometer. Solid UV-vis spectra were recorded on a JASCO V-770 Spectrophotometer within the wavelength range of 200-800 nm. Thermogravimetric analysis (TGA) was recorded on a TG-DTA8122 thermal analyzer with a N_2 flow rate of 30 mL min^{-1} at a heating rate of 5 °C min^{-1} from room temperature to 800 °C. Powder X-ray diffraction (PXRD) data were collected

 doi:10.20944/preprints202407.1981.v1

on a Rigaku Smart Lab powder diffractometer using a Cu Kα source (λ = 1.5418 Å) over the range of 2θ = 2.0 - 30.0° with a step size of 0.02° and 2 s per step. The sorption isotherms for N_2 were measured by using a MICROTRAC MRB BELSORP MAX II analyzer with ultra-high-purity gas (99.999% purity). To estimate the pore size distributions, nonlocal density functional theory (NLDFT) was applied to analyze the N_2 isotherm on the basis of the model of N_2@77K on carbon with slit pores and the method of non-negative regularization. The scanning electron microscopy (SEM) images were obtained on thermoscientific Verios G4 UC scanning electron microscope. Low-dose high-resolution transmission electron microscopy (HRTEM) was performed on a thermoscientific Talos F200X G2. The photoluminescence spectroscopy (PL) was collected on a JASCO FP-8600. The fluorescence lifetime was collected on a Quantaurus-Tau C16361.

3. Results and Discussion

3.1. Synthesis and Characterization of COFs

A novel benzoselenadiazole-based imine-linked framework, designated as TPE-BSD-COF, was successfully synthesized through the condensation reaction between TPE and BSD monomers (Figure 1 and Figure S1). The solvothermal synthesis was carried out in a mixed solvent of o-dichlorobenzene and 1-butanol, with acetic acid (6 M) as catalyst at 120 °C, over 72 hours. Upon completion, a yellow powder was produced with a yield of 79%. The detailed synthesis procedure was provided in the Supporting Information.

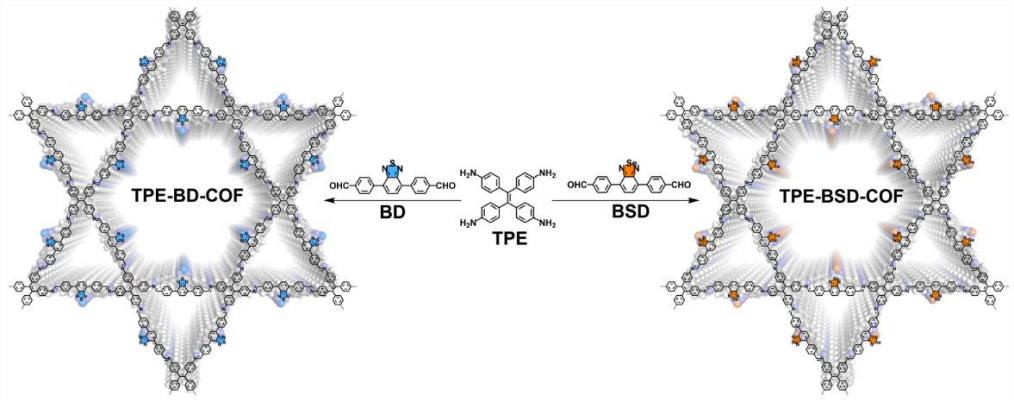

Figure 1. Schematic diagram of synthesized TPE-BSD-COF and TPE-BD-COF.

The similar synthesis method has been used to synthesize TPE-BD-COF (Figure 1 and Figure S2). Powder X-ray diffraction (PXRD) analysis revealed that both TPE-BSD-COF and TPE-BD-COF are crystalline porous materials (Figure 2a and Figure S3a). The PXRD pattern of TPE-BSD-COF exhibits a significant peak at 1.82°, as well as smaller peaks at 3.15°, 3.64°, and 4.82°, corresponding to the (100), (110), (200), and (300) reflections, respectively. The experimental PXRD pattern of TPE-BSD-COF corresponded well with the curve calculated in AA stacking mode (Figure 2a purple line, Figure 2b and Figure S4). For TPE-BSD-COF, the Pawley refined lattice parameters were $a = b$ = 55.98 Å, c = 5.04 Å, and $\alpha = \beta = \gamma$ = 90°; the corresponding R_{wp} and R_p values were 4.80% and 3.06%, respectively. TPE-BD-COF exhibits distinct peaks at 1.82°, 3.64°, 4.82°, 5.46°, 6.57°, 7.29°, 9.47°, and approximately 20.06°, corresponding to the (100), (200), (120), (300), (130), (400), (330), and (001) facets, respectively. These findings align well with the PXRD results obtained from the simulations in the AA stacking mode (Figure S3a, blue line, Figure S3b and Figure S5). The TPE-BD-COF Pawley refined lattice parameters were $a = b$ = 55.98 Å, c = 5.04 Å, and $\alpha = \beta = \gamma$ = 90°, with R_{wp} = 5.17% and R_p = 3.24% as refinement results.

Fourier transform infrared spectroscopy (FT-IR) and solid-state ^{13}C cross-polarized magic angle spinning nuclear magnetic resonance (^{13}C CP/MAS NMR) spectroscopy verified the existence of TPE-BSD-COF and TPE-BD-COF. In their FT-IR spectra, the distinctive vibrational peak of -CHO at 1696 cm^{-1} was noticeably diminished after the condensation reaction. Meanwhile, TPE-BSD-COF exhibited

 doi:10.20944/preprints202407.1981.v1

a prominent stretching signal at 1626 cm^{-1}, which can be attributed to the C=N moiety, indicating the successful formation of the imine bonds (Figure 2c). A similar phenomenon was also observed by TPE-BD-COF (Figure S3c). Furthermore, based on Figure 2d and Figure S3d, the chemical shifts at 164.18 ppm (TPE-BSD-COF) and 160.20 ppm (TPE-BD-COF) are attributed to the imine carbons. Additionally, the peaks of TPE-BSD-COF at 158.67 and 151.12 ppm, as well as the peaks of TPE-BD-COF at 153.30 and 148.96 ppm, are specifically associated with benzoselenadiazole and benzothiadiazole units. The broader peaks observed at 110.25-140.90 ppm in both COFs are related to the carbons present in the benzene ring. Measurements using X-ray photoelectron spectroscopy (XPS) were then performed to obtain insights into the elemental composition and valence states of the COFs. Examination of the XPS survey spectra of TPE-BSD-COF and TPE-BD-COF revealed the presence of Se and S elements, in addition to C, N, and O elements (Figure 2e and Figure S3e). This confirms the successful incorporation of benzoselenadiazole and benzothiadiazole into the frameworks of TPE-BSD-COF and TPE-BD-COF, respectively. In the case of TPE-BSD-COF, the Se 3d spectra showed binding energies around 57.5 and 58.3 eV, which correspond to the Se 3d 5/2 and Se 3d 3/2 peaks of the benzoselenadiazole unit (Figure 2f). [41] The S 2p spectra in TPE-BD-COF displayed S binding energies at approximately 165.8 and 167.0 eV, which can be attributed to the S 2p 3/2 and S 2p 1/2 of the benzothiadiazole unit, respectively (Figure S3f). [42]

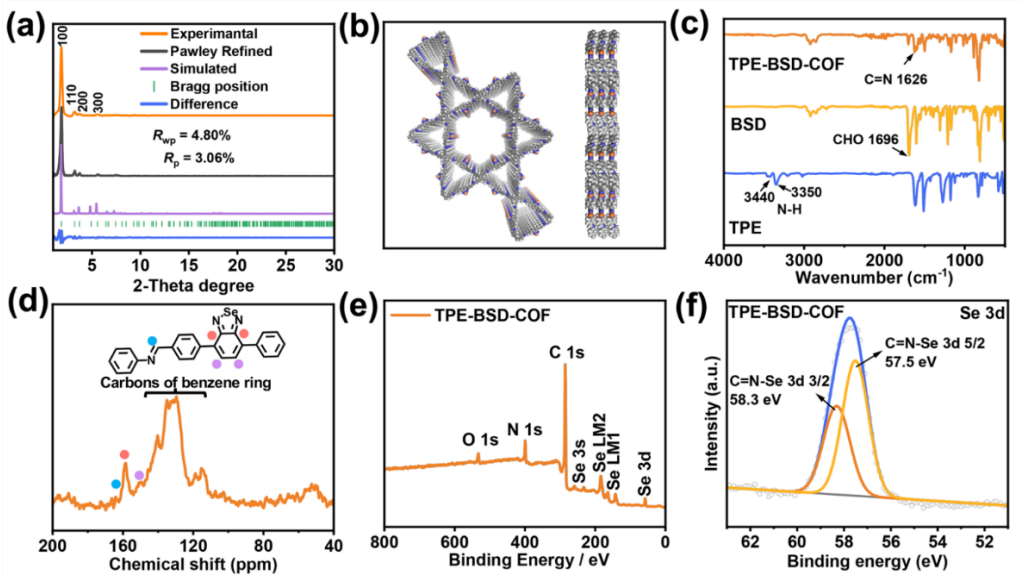

Figure 2. The experimental and simulated PXRD patterns of TPE-BSD-COF (a). Structural model of TPE-BSD-COF (b). FT-IR spectra of TPE-BSD-COF and the monomers (c). Solid-state ^{13}C CP/MAS NMR spectra of TPE-BSD-COF (d). Survey-scan XPS spectrum (e) and High-resolution Se 3d XPS spectrum (f) of TPE-BSD-COF.

Figure 3a and Figure S6a illustrate the Brunauer–Emmett–Teller (BET) surface areas of TPE-BSD-COF and TPE-BD-COF as 190 and 1040 $m^2\ g^{-1}$, respectively. Both COFs display typical type IV isotherms, indicating their porous nature. The pore widths of TPE-BSD-COF, analyzed using nonlocal density functional (NLDFT), are centered at 1.7 and 3.4 nm for TPE-BSD-COF (Figure 3b) and 1.7 and 4.1 nm (Figure S6b) for TPE-BD-COF, respectively. These findings align with the simulated AA layer structure.

High-resolution scanning electron microscopy (HR-SEM) and high-resolution transmission electron microscopy (HR-TEM) were used to examine the morphology of the two COFs. As shown in Figure 3c and Figure S6c, both COFs exhibit a rod-like morphology with a diameter of about 2 μm. HR-TEM images of TPE-BSD-COF and TPE-BD-COF showed clear lattice fringes, indicating long-range ordered channels, further illustrating their high crystallinity (Figure 3d and Figure S6d). The thermal stability of the two COFs was assessed through thermogravimetric analysis (TGA). Both

 doi:10.20944/preprints202407.1981.v1

COFs demonstrated exceptional thermal stability above 500 °C, with a weight loss of less than 5%, as illustrated in Figure S7.

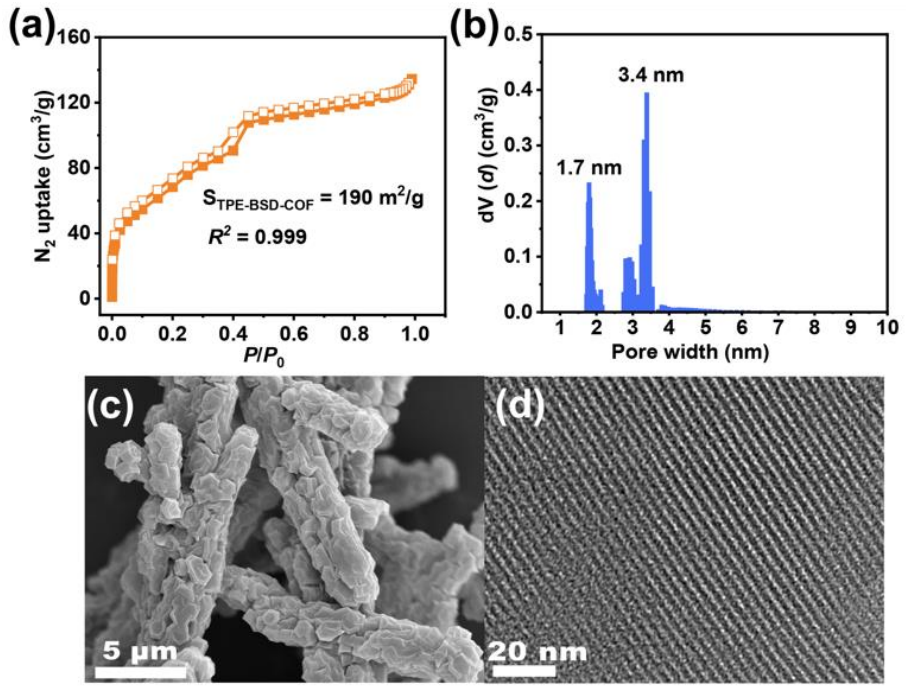

Figure 3. Nitrogen adsorption isotherm (a), pore size distribution (b), HR-SEM image (c) and HR-TEM image (d) of TPE-BSD-COF.

3.2. Photophysical/Electrochemical Properties

Before investigating the suitability of TPE-BSD-COF and TPE-BD-COF for photocatalytic organic conversion, we compared their photoelectric properties. The optical absorption properties were analyzed using solid-state UV-visible diffuse reflectance spectroscopy. Figure 4a illustrates that the light absorption ranges of the two COFs are notably broader than those of the monomers, extending beyond 525 nm. This expansion is primarily attributed to the conjugated system of the COFs material. Specifically, the light absorption range of TPE-BSD-COF is red-shifted by approximately 20 nm compared to TPE-BD-COF, suggesting a wider absorption range. The optical bandgaps of both COFs were calculated using Tauc diagrams, resulting in bandgaps of 2.00 eV for TPE-BSD-COF and 2.06 eV for TPE-BD-COF (Figure 4b). Mott-Schottky measurements determined the conduction band minimum (CBM) of -1.31 V vs NHE for TPE-BSD-COF and -1.42 V vs NHE for TPE-BD-COF, as shown in Figure 4c. According to the formula Eg = EVB - ECB, the valence band maxima (VBM) of TPE-BSD-COF and TPE-BD-COF is estimated to be 0.69 and 0.64 V (vs NHE), respectively. The band structure arrangement is illustrated in Figure 4d. Time-resolved fluorescence decay spectroscopy was performed on TPE-BSD-COF and TPE-BD-COF. The data, depicted in Figure 4e and Table S3, demonstrated an average lifetime of 0.96 ns for TPE-BSD-COF and 0.73 ns for TPE-BD-COF. This increased lifetime observed in TPE-BSD-COF implies better charge carrier separation compared to TPE-BD-COF, which indicates superior photocatalytic performance of the former. [43] In addition, the EIS Nyquist diagram (Figure 4f) demonstrates that the semicircle diameter of TPE-BSD-COF is reduced compared to TPE-BD-COF. This observation implies that photogenerated charge carriers in TPE-BSD-COF are transported and separated more efficiently, resulting in a more proficient limitation of electron-hole recombination. [44]

 doi:10.20944/preprints202407.1981.v1

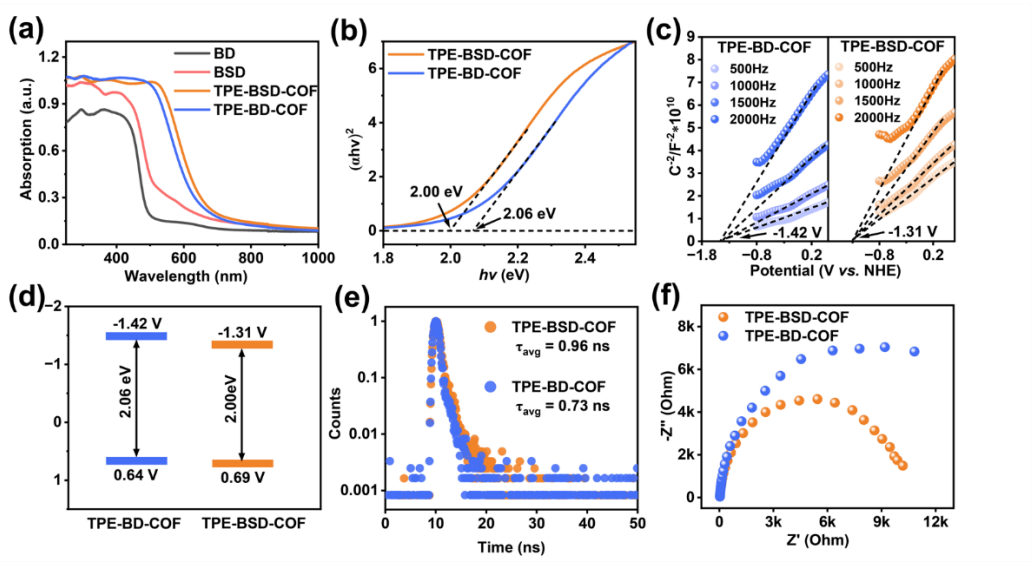

Figure 4. UV–vis spectra of BD, BSD, TPE-BD-COF, and TPE-BSD-COF (a). The optical band gap of TPE-BD-COF and TPE-BSD-COF identified using the Tauc plot (b). Mott–Schottky plots of TPE-BD-COF and TPE-BSD-COF (c). Energy band structures of TPE-BD-COF and TPE-BSD-COF (d). Time-resolved PL spectra of TPE-BD-COF and TPE-BSD-COF (e). EIS Nyquist plots of TPE-BD-COF and TPE-BSD-COF (f).

3.3. Photocatalytic Performance and Possible Mechanisms

By combining the optical band gap, energy level arrangement, and Electrochemical impedance spectra (EIS) results of the two COFs, it can be inferred that TPE-BSD-COF and TPE-BD-COF exhibit photocatalytic activity for the reductive dehalogenation of benzoyl bromide derivatives. Optimizing the reaction conditions involved using *α*-bromoacetophenone (1a) as the standard substrate, TPE-BSD-COF, and TPE-BD-COF as the photocatalyst, *N,N*-diisopropylethylamine (DIPEA) as the deacid agent, electron donor, and source of hydrogen (Figure 5a). After being exposed to a blue LED lamp (460-465 nm, 25 W) for 1 hour in the presence of DMF as the solvent, the yield of acetophenone (2a) achieved 98% and 95%. In contrast, the yield decreased when acetonitrile (CH_3CN) and tetrahydrofuran (THF) were used as solvents, respectively. Only a limited range of products can be identified in the absence of COFs, DIPEA, or light settings, showcasing their collective impact on the photocatalytic mechanism. Seven additional compounds with either electron-donating or electron-withdrawing substituents were examined to evaluate the viability of the debromination method for various *α*-bromoacetophenone derivatives (Figure 5b). The results showed that substituents that either donate or withdraw electrons did not significantly affect the rate of the debromination reaction, and the resulting yields of products (2b-2h) stayed at high levels. Cycling experiments were conducted to assess the structural stability of TPE-BSD-COF after photocatalysis. The results showed that the TPE-BSD-COF catalyst was able to maintain its structural integrity after undergoing repeated filtration, washing, and drying processes. Additionally, the yield of the products remained consistent even after five cycles of use, indicating that the TPE-BSD-COF catalyst is durable and can be easily separated and reused multiple times without a significant decrease in performance (Figure 5c). PXRD and SEM analyses further validated the preservation of crystallinity and structural integrity of TPE-BSD-COF after five rounds of photocatalytic cycling, indicating that TPE-BSD-COF exhibits remarkable stability (Figure S8).

Preprints.org (www.preprints.org) | NOT PEER-REVIEWED | Posted: 25 July 2024 doi:10.20944/preprints202407.1981.v1

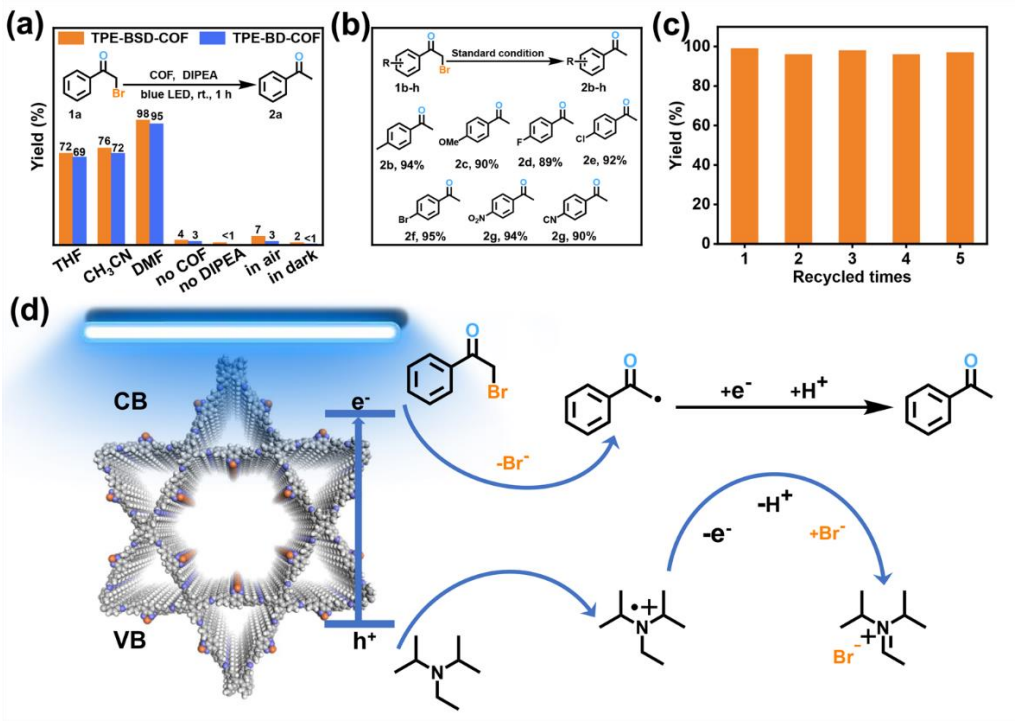

Figure 5. Variations of reaction conditions: **1a** (0.4 mmol), DIPEA (120 mg, 0.88 mmol), COFs (6 mg), solvent (1 mL), and 18 W blue LED in a N_2 environment at room temperature for 1 hour. Yield based on **1a** (a). The substrate range for α-bromoacetophenone analogues (b). Recycling of TPE-BSD-COF in photocatalytic debromination of **1a** (c). Schematic diagram of photocatalytic debromination reaction mechanism (d).

Drawing from existing studies, [45] a potential mechanism for the debromination process of α-bromoacetophenone was suggested, illustrated in Figure 5d. Under the illumination of LED light, the photogenerated electrons are transferred from the conduction band of TPE-BSD-COF or TPE-BD-COF to α-bromoacetophenone, forming an α-carbonyl radical and a bromide anion. The α-carbonyl radical then abstracts an H^+ and electrons from DIPEA, leading to the production of acetophenone. In this reaction, DIPEA serves both as a hydrogen source and a deacidifying reagent, forming a by-product.

5. Conclusions

In summary, two benzodiazole-based heteropore COFs, i.e., benzoselenadiazole-containing TPE-BSD-COF and benzothiadiazole-containing TPE-BD-COF, have been successfully designed and constructed by imine condensation reaction under solvothermal conditions. Both COFs exhibit strong crystallinity, an inherent pore structure, excellent photovoltaic performance, and remarkable photocatalytic durability. These characteristics suggest that the materials have clearly defined crystalline structures that show a natural capacity to incorporate pores within their framework, efficiently convert light into electricity, and can endure extended exposure to photocatalytic reactions. Both TPE-BSD-COF and TPE-BD-COF exhibit excellent photoelectric characteristics such as an extensive light absorption spectrum, reduced optical bandgap, minimal EIS, and long fluorescence lifetime. These traits indicate that the two COFs possess strong charge-transferring and separation abilities, leading to improved performance in photocatalytic debromination ability for α-bromoacetophenone. Among them, the new TPE-BSD-COF achieved a photocatalytic yield of 98% in only 1 hour. This study not only expands the variety of COFs, but also demonstrates their potential as photocatalysts for the photocatalytic dehalogenation reaction of phenylacetyl bromide

derivatives. This serves as an important reference for COFs synthesis as well as for exploring the heterogeneous photocatalysis exhibited by COFs.

Supplementary Materials: The following supporting information can be downloaded at the website of this paper posted on Preprints.org, Figure S1: title; Table S1: title; Video S1: title.

Author Contributions: Conceptualization, M.W. and Y.G.; methodology, J.Q.; software, H.H.; validation, M.W., Z.W. and S.W.; formal analysis, S.W. and S.X.; investigation, M.W.; resources, Y.G.; data curation, M.W.; writing—original draft preparation, M.W.; writing—review and editing, S.X.; visualization, J.Q.; supervision, Y.G.; project administration, Y.G.; funding acquisition, Y.Y. All authors have read and agreed to the published version of the manuscript."

Funding: This work was supported by the Major Science and Technology Plan of Hainan Province, China (ZDKJ202016), the Key Research and Development Project of Hainan Province, China (ZDYF2024GXJS005) and the National Natural Science Foundation of China (21965011).

Institutional Review Board Statement: Not applicable.

Data Availability Statement: The data presented in this study are available on request from the corresponding author.

Conflicts of Interest: The authors declare no conflicts of interest.

References

1. Parvatkar, P.T.; Kandambeth, S.; Shaikh, A.C.; Nadinov, I.; Yin, J.; Kale, V.S.; Healing, G.; Emwas, A.-H.; Shekhah, O.; Alshareef, H.N.; et al. A Tailored COF for Visible-Light Photosynthesis of 2,3-Dihydrobenzofurans. *J. Am. Chem. Soc.* **2023**, *145*, 5074–5082, doi:10.1021/jacs.2c10471.
2. Liu, Z.; Chen, Z.; Tong, H.; Ji, M.; Chu, W. A β-Ketoenamine-Linked Covalent Organic Framework as a Heterogeneous Photocatalyst for the Synthesis of 2-Arylbenzothiazoles by Cyclization Reaction. *Green Chem.* **2023**, *25*, 5195–5205, doi:10.1039/D3GC00721A.
3. Yuan, L.; Qi, M.-Y.; Tang, Z.-R.; Xu, Y.-J. Coupling Strategy for CO_2 Valorization Integrated with Organic Synthesis by Heterogeneous Photocatalysis. *Angew. Chem. Int. Edi.* **2021**, *60*, 21150–21172, doi:10.1002/anie.202101667.
4. Ma, J.; Miao, T.J.; Tang, J. Charge Carrier Dynamics and Reaction Intermediates in Heterogeneous Photocatalysis by Time-Resolved Spectroscopies. *Chem. Soc. Rev.* **2022**, *51*, 5777–5794, doi:10.1039/D1CS01164B.
5. Liras, M.; Barawi, M.; O'Shea, V.A. de la P. Hybrid Materials Based on Conjugated Polymers and Inorganic Semiconductors as Photocatalysts: From Environmental to Energy Applications. *Chem. Soc. Rev.* **2019**, *48*, 5454–5487, doi:10.1039/C9CS00377K.
6. Friedmann, D.; Lee, A.F.; Wilson, K.; Jalili, R.; Caruso, R.A. Printing Approaches to Inorganic Semiconductor Photocatalyst Fabrication. *J. Mater. Chem. A* **2019**, *7*, 10858–10878, doi:10.1039/C9TA00888H.
7. Hoffman, E.; Kozakiewicz, K.; Rybczyńska, M.; Mońka, M.; Grzywacz, D.; Liberek, B.; Bojarski, P.; Serdiuk, I.E. Photochemical Transformation of a Perylene Diimide Derivative Beneficial for the in Situ Formation of a Molecular Photocatalyst of the Hydrogen Evolution Reaction. *J. Mater. Chem. A* **2024**, *12*, 5233–5243, doi:10.1039/D3TA05930H.
8. Rana, P.; Singh, N.; Majumdar, P.; Prakash Singh, S. Evolution of BODIPY/Aza-BODIPY Dyes for Organic Photoredox/Energy Transfer Catalysis. *Coordin Chem Rev* **2022**, *470*, 214698, doi:10.1016/j.ccr.2022.214698.
9. Ekande, O.S.; Kumar, M. Review on Polyaniline as Reductive Photocatalyst for the Construction of the Visible Light Active Heterojunction for the Generation of Reactive Oxygen Species. *J. Environ. Chem. Eng.* **2021**, *9*, 105725, doi:10.1016/j.jece.2021.105725.
10. Shi, X.; Yu, Y.; Yang, Q.; Hong, X. Carboxyl Groups as Active Sites for H_2O_2 Decomposition in Photodegradation over Graphene Oxide/Polythiophene Composites. *App. Surf. Sci.* **2020**, *524*, 146397, doi:10.1016/j.apsusc.2020.146397.
11. Zong, X.; Miao, X.; Hua, S.; An, L.; Gao, X.; Jiang, W.; Qu, D.; Zhou, Z.; Liu, X.; Sun, Z. Structure Defects Assisted Photocatalytic H_2 Production for Polythiophene Nanofibers. *Appl. Catal. B Environ.* **2017**, *211*, 98–105, doi:10.1016/j.apcatb.2017.04.033.
12. Guo, L.; Gao, J.; Huang, Q.; Wang, X.; Li, Z.; Li, M.; Zhou, W. Element Engineering in Graphitic Carbon Nitride Photocatalysts. *Renew Sust Energ Rev* **2024**, *199*, 114482, doi:10.1016/j.rser.2024.114482.

13. Cao, S.; Low, J.; Yu, J.; Jaroniec, M. Polymeric Photocatalysts Based on Graphitic Carbon Nitride. *Adv. Mater.* **2015**, *27*, 2150-2176, doi:10.1002/adma.201500033.
14. Li, Y.; Yan, S.; Jia, X.; Wu, J.; Yang, J.; Zhao, C.; Wang, S.; Song, H.; Yang, X. Uncovering the Origin of Full-Spectrum Visible-Light-Responsive Polypyrrole Supramolecular Photocatalysts. *Appl. Catal. B Environ.* **2021**, *287*, 119926, doi:10.1016/j.apcatb.2021.119926.
15. Lin, H.; Yang, Y.; Festus, K.W.; Hsu, Y.-C.; Liang, R.-R.; Afolabi, I.; Zhou, H.-C. Integrating Photoactive Ligands into Dimension-Reduced Metal–Organic Frameworks: Harnessing the Power of Organic Photocatalysts. *Acc. Mater. Res.* **2024**, *5*, 236–248, doi:10.1021/accountsmr.3c00144.
16. Xu, W.; Zhang, G.-R.; Wang, J.; Yu, H.; Zhang, W.; Shen, L.-L.; Mei, D. Enhanced Intermolecular Electron Transfer in Fluorinated Metal–Organic Framework Photocatalysts for Efficient CO_2 Reduction. *Adv. Funct. Mater*. **2024**, *34*, 2312691, doi:10.1002/adfm.202312691.
17. Han, X.; Wu, H.; Chen, S.; Deng, S.; Wang, J. Novel Layer-to-Layer Charge Transfer in an Anion-Pillared Metal-Organic Framework for Efficient CO_2 Photoreduction to CH_4. *Chem. Eng. J.* **2024**, *479*, 147694, doi:10.1016/j.cej.2023.147694.
18. Tian, Y.; Zhu, G. Porous Aromatic Frameworks (PAFs). *Chem. Rev.* **2020**, *120*, 8934–8986, doi:10.1021/acs.chemrev.9b00687.
19. Cao, L.; Wang, C.; Wang, H.; Xu, X.; Tao, X.; Tan, H.; Zhu, G. Rationally Designed Cyclooctatetrathiophene-Based Porous Aromatic Frameworks (COTh-PAFs) for Efficient Photocatalytic Hydrogen Peroxide Production. *Angew. Chem. Int. Edi.* **2024**, *63*, e202402095, doi:10.1002/anie.202402095.
20. Segura, J.L.; Royuela, S.; Ramos, M.M. Post-Synthetic Modification of Covalent Organic Frameworks. *Chem. Soc. Rev.* **2019**, *48*, 3903–3945, doi:10.1039/C8CS00978C.
21. Qian, C.; Teo, W.L.; Gao, Q.; Wu, H.; Liao, Y.; Zhao, Y. Polycrystalline Covalent Organic Frameworks. *Mater. Today* **2023**, *71*, 91–107, doi:10.1016/j.mattod.2023.11.005.
22. Yang, Q.; Luo, M.; Liu, K.; Cao, H.; Yan, H. Covalent Organic Frameworks for Photocatalytic. *Appl. Catal. B Environ.* **2020**, *276*, 119174, doi:10.1016/j.apcatb.2020.119174.
23. Medina, D.D.; Sick, T.; Bein, T. Photoactive and Conducting Covalent Organic Frameworks. *Adv. Energy Mater*. **2017**, *7*, 1700387, doi:10.1002/aenm.201700387.
24. Li, R.; Tang, X.; Wu, J.; Zhang, K.; Zhang, Q.; Wang, J.; Zheng, J.; Zheng, S.; Fan, J.; Zhang, W.; et al. A Sulfonate-Functionalized Covalent Organic Framework for Record-High Adsorption and Effective Separation of Organic Dyes. *Chem. Eng. J.* **2023**, *464*, 142706, doi:10.1016/j.cej.2023.142706.
25. Liu, M.; Xu, Q.; Zeng, G. Ionic Covalent Organic Frameworks in Adsorption and Catalysis. *Angew. Chem. Int. Edi.* **2024**, *63*, e202404886, doi:10.1002/anie.202404886.
26. Gong, C.; Yan, C.; Liu, J.; Li, J.; Fu, J.; Chen, C.; Huang, Y.; Yuan, G.; Peng, Y. Insights into Sensing Applications of Fluorescent Covalent Organic Frameworks. *Trac-trend Anal Chem* **2024**, *173*, 117625, doi:10.1016/j.trac.2024.117625.
27. Wu, X.; Han, X.; Xu, Q.; Liu, Y.; Yuan, C.; Yang, S.; Liu, Y.; Jiang, J.; Cui, Y. Chiral BINOL-Based Covalent Organic Frameworks for Enantioselective Sensing. *J. Am. Chem. Soc.* **2019**, *141*, 7081–7089, doi:10.1021/jacs.9b02153.
28. Hegazy, H.H.; Sana, S.S.; Ramachandran, T.; Kumar, Y.A.; Kulurumotlakatla, D.K.; Abd-Rabboh, H.S.M.; Kim, S.C. Covalent Organic Frameworks in Supercapacitors: Unraveling the Pros and Cons for Energy Storage. *J. Energy Storage.* **2023**, *74*, 109405, doi:10.1016/j.est.2023.109405.
29. Alsudairy, Z.; Brown, N.; Campbell, A.; Ambus, A.; Brown, B.; Smith-Petty, K.; Li, X. Covalent Organic Frameworks in Heterogeneous Catalysis: Recent Advances and Future Perspective. *Mater. Chem. Front.* **2023**, *7*, 3298–3331, doi:10.1039/D3QM00188A.
30. Guo, J.; Jiang, D. Covalent Organic Frameworks for Heterogeneous Catalysis: Principle, Current Status, and Challenges. *ACS Cent. Sci.* **2020**, *6*, 869–879, doi:10.1021/acscentsci.0c00463.
31. Wang, X.; Han, X.; Zhang, J.; Wu, X.; Liu, Y.; Cui, Y. Homochiral 2D Porous Covalent Organic Frameworks for Heterogeneous Asymmetric Catalysis. *J. Am. Chem. Soc.* **2016**, *138*, 12332–12335, doi:10.1021/jacs.6b07714.
32. Keller, N.; Bein, T. Optoelectronic Processes in Covalent Organic Frameworks. *Chem. Soc. Rev.* **2021**, *50*, 1813–1845, doi:10.1039/D0CS00793E.
33. Liu, Z.; Yang, X.; Yang, Z.; Su, X.; Xie, Z.; Chen, W.; Zhang, W.; Chen, L. Quinacridone Based 2D Covalent Organic Frameworks as Efficient Photocatalysts for Aerobic Oxidative Povarov Reaction. *Appl. Catal. B Environ.* **2022**, *312*, 121406, doi:10.1016/j.apcatb.2022.121406.

34. Stegbauer, L.; Schwinghammer, K.; Lotsch, B.V. A Hydrazone-Based Covalent Organic Framework for Photocatalytic Hydrogen Production. *Chem. Sci.* **2014**, *5*, 2789–2793, doi:10.1039/C4SC00016A.
35. Chen, R.; Shi, J.-L.; Ma, Y.; Lin, G.; Lang, X.; Wang, C. Designed Synthesis of a 2D Porphyrin-Based sp2 Carbon-Conjugated Covalent Organic Framework for Heterogeneous Photocatalysis. *Angew. Chem. Int. Edi.* **2019**, *58*, 6430–6434, doi:10.1002/anie.201902543.
36. Verma, K.; Addicoat, M.A.; Justin Thomas, K.R. Carbazole-Based Imine-Linked Covalent Organic Framework for Efficient Heterogeneous Photocatalysis. *ACS Appl. Polym. Mater.* **2024**, *6*, 3909–3917, doi:10.1021/acsapm.3c03207.
37. Dash, B.P.; Hamilton, I.; Tate, D.J.; Crossley, D.L.; Kim, J.-S.; Ingleson, M.J.; Turner, M.L. Benzoselenadiazole and Benzotriazole Directed Electrophilic C–H Borylation of Conjugated Donor-Acceptor Materials. *J. Mater. Chem. C* **2019**, *7*, 718–724, doi:10.1039/C8TC05131C.
38. Yue, J.-Y.; Wang, Y.-T.; Ding, X.-L.; Fan, Y.-F.; Song, L.-P.; Yang, P.; Ma, Y.; Tang, B. Single-Atom Substitution in Donor-Acceptor Covalent Organic Frameworks for Tunable Visible Light Photocatalytic Cr(VI) Reduction. *Mater. Chem. Front.* **2022**, *6*, 3748–3754, doi:10.1039/D2QM00880G.
39. Yang, F.; Li, X.; Qu, H.-Y.; Kan, J.-L.; Guo, Y.; Dong, Y.-B. A Selenium Atom Involved Covalent Organic Framework for Window Ledge Photocatalytic Oxidation of Sulfides. *Chin. J. Chem.* doi:10.1002/cjoc.202400139.
40. Liang, R.-R.; Jiang, S.-Y.; A, R.-H.; Zhao, X. Two-Dimensional Covalent Organic Frameworks with Hierarchical Porosity. *Chem. Soc. Rev.* **2020**, *49*, 3920–3951, doi:10.1039/D0CS00049C.
41. Li, P.; Ge, F.; Yang, Y.; Wang, T.; Zhang, X.; Zhang, K.; Shen, J. 1D Covalent Organic Frameworks Triggering Highly Efficient Photosynthesis of H_2O_2 via Controllable Modular Design. *Angew. Chem. Int. Edi.* **2024**, *63*, e202319885, doi:10.1002/anie.202319885.
42. Deng, M.; Wang, L.; Wen, Z.; Chakraborty, J.; Sun, J.; Wang, G.; Voort, P.V.D. Donor-Acceptor sp2 Covalent Organic Frameworks for Photocatalytic H_2O_2 Production and Tandem Bisphenol-A Degradation. *Green Chem.* **2024**, *26*, 3239–3248, doi:10.1039/D3GC04045C.
43. Wang, T.; Li, M.; Chen, Y.; Che, X.; Bi, F.; Yang, Y.; Yang, R.; Li, C. Regioisomeric Benzotriazole-Based Covalent Organic Frameworks for High Photocatalytic Activity. *ACS Catal.* **2023**, *13*, 15439–15447, doi:10.1021/acscatal.3c04145.
44. Yang, C.; Zhang, Z.; Li, J.; Hou, Y.; Zhang, Q.; Li, Z.; Yue, H.; Liu, X. Benzotrifuran-Based Donor-Acceptor Covalent Organic Frameworks for Enhanced Photocatalytic Hydrogen Generation. *Green Chem.* **2024**, *26*, 2605–2612, doi:10.1039/D3GC04972H.
45. Liu, H.; Li, C.; Li, H.; Ren, Y.; Chen, J.; Tang, J.; Yang, Q. Structural Engineering of Two-Dimensional Covalent Organic Frameworks for Visible-Light-Driven Organic Transformations. *ACS Appl. Mater. Interfaces* **2020**, *12*, 20354–20365, doi:10.1021/acsami.0c00013.